

Optical design of the SCUBA-2 IFTS

Melanie R. Leclerc^{*a}, Brad Gom^b, David Naylor^b

^aINO, 2740 Einstein, Quebec, Quebec, Canada, G1P 4S4

^bPhysics Department, University of Lethbridge, Lethbridge, Alberta, Canada, T1K 3M4

ABSTRACT

An Imaging Fourier Transform Spectrometer (IFTS), named FTS-2, is being developed by the University of Lethbridge for use with the SCUBA-2 sub-millimeter bolometric camera on the James Clerk Maxwell Telescope (JCMT). The FTS-2 optical model was developed and optimized in Zemax by the Institut National d'Optique (INO) to maximize the FOV and efficiency over a range of spectral resolutions. The IFTS has been designed as a folded system including corner cubes in the interferometer moving mirror, and extended polynomial surfaces in the interferometer folding mirrors. The instrument design for FTS-2 is described elsewhere; here we present an analysis of the modeled performance of the IFTS in terms of achievable Field Of View (FOV), spot pattern and vignetting, at Zero Path Difference (ZPD) and for the 2 resolution modes. The predicted imaging performance is compared to that of the SCUBA-2 camera alone.

Keywords: SCUBA-2, JCMT, IFTS, imaging, spectrometer, sub-millimeter, optical design, Zemax

1. INTRODUCTION

The Submillimetre Common User Bolometer Array instrument (SCUBA)¹ on the James Clerk Maxwell Telescope (JCMT) has made significant contributions to wide range of astronomical problems from the study of galaxy formation and evolution in the early Universe to star and planet formation in our own Galaxy. These pioneering accomplishments provided the impetus for the development of SCUBA-2, a revolutionary new large format submillimeter camera², which has recently been delivered to the JCMT. SCUBA-2 features two dc-coupled, monolithic TES filled arrays operating at 450 and 850 μm with a total of $\sim 10,000$ bolometers, unlike previous detectors which have used much smaller arrays of discrete bolometers. With its larger format and increased sensitivity, SCUBA-2 promises a factor of 1000 increase in mapping speed compared to its predecessor. Two ancillary instruments, a polarimeter and imaging spectrometer, are also being developed to further extend the capabilities of SCUBA-2. A Fourier Transform Spectrometer (FTS) was selected as the optimal intermediate resolution spectrometer for SCUBA-2. The instrument, named FTS-2, will be primarily a galactic spectrometer (e.g. spectral index mapping of molecular clouds), but will also provide useful information on bright nearby galaxies and planetary atmospheres. FTS-2 thus fills a niche between the dual band SCUBA-2 continuum images and the higher spectral resolution, but smaller images produced by the JCMT heterodyne facility instrument HARP-B. In this paper we present details of the optical design of FTS-2; the instrument design and observing issues are presented elsewhere.³

Since the layout of the JCMT - SCUBA-2 feed optics was well advanced prior to the decision to include a spectrometer, the mechanical, optical, and software design of FTS-2 was significantly more challenging. The only practical location to mount an FTS is at the exit of the JCMT telescope elevation bearing, midway through the SCUBA-2 feed optics, as shown in Fig. 1. The FTS-2 optics were initially modeled in Zemax by the University of Lethbridge as a folded system of paraxial mirrors⁴; the design was subsequently optimized by INO. Each mirror surface shape and position was optimized based on a set of criteria provided by the University of Lethbridge, namely a minimum clearance to leave space for the telescope beam when FTS-2 is not in use, the available volume, and the location of the base plate below the telescope beam optical axis. For compatibility with normal photometric data collected with SCUBA-2, it is necessary to minimize the impact of the interferometer on the image spot size, magnification and FOV, for all resolution modes. Within the interferometer, the beams at the corner cubes must be collimated, there must be pupils located at the corner cubes for symmetry, and the beam waist near the beam splitters must be minimized to reduce the beamsplitter diameters. Design goals included maximizing the useable FOV, and providing spectral resolution from 0.1 to 0.006 cm^{-1} .

* Melanie.Leclerc@ino.ca; phone 1 418 657-7006; fax 1 418 657-7009; ino.ca

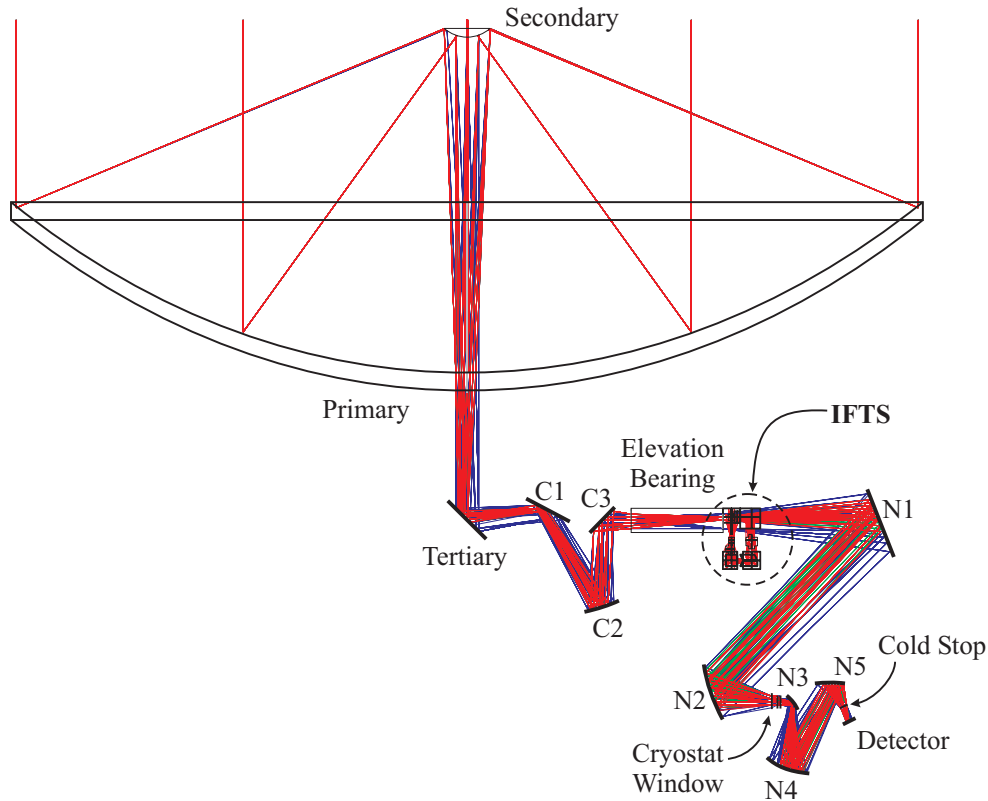


Fig. 1. The IFTS is located between the JCMT elevation bearing and mirror N1. The SCUBA-2 feed optics consist of 3 mirrors in the receiver cabin (C1 to C3), 2 mirrors on the Nasmyth level (N1 and N2), and 3 mirrors inside the SCUBA-2 cryostat (N3 to N5).

2. METHODOLOGY

Starting from the original IFTS design, the paraxial mirrors were replaced by real mirrors (extended polynomials) and the rooftop mirrors were replaced by hollow corner cubes. Corner cubes placed back-to-back with nearly coinciding apices eliminate any tilt and shear introduced by the translation stage, but more importantly, also provide proper parity of the reflections in the vertically folded design. An analysis of the performances of the IFTS was performed, and the results are presented below. We detail the performances in terms of achievable FOV, spot pattern and vignetting, at ZPD and for the 2 resolution modes of 0.1 and 0.006 cm^{-1} (3 GHz and 180 MHz) corresponding to displacements of the translation stage of $\pm 15 \text{ mm}$ and $\pm 200 \text{ mm}$, respectively. We compare the performance of the camera alone with that of the camera coupled to the spectrometer. A view of FTS-2 on its planned mounting location is shown in Fig. 2.

It is important that all optical and mechanical components are located so as to not interfere with the SCUBA-2 beam when the interferometer is not in use. A key feature is a translation mechanism which allows the four pick-off mirrors to slide horizontally into and out of the beam, so that when extracted there is sufficient space between the pick-off mirrors and the upper folding mirrors to allow the telescope beam through during normal photometric observations. The beamsplitters (BS1 and BS2) are mounted on the mechanically damped base plate; additional clearance was provided to accommodate the beam splitter mounting rings (which add $\sim 10 \text{ mm}$ to the clear aperture radius) and allow $\sim 40 \text{ mm}$ clearance between the telescope beam and the second beam splitter (see Fig. 3). The design also meets the requirement of available volume, limited by the base plate that is positioned 772 mm below the telescope optical axis, and by the backing structure of the primary mirror which passes close to the spectrometer framework when the dish points to the horizon. There could obviously also be no mechanical interference between folding mirrors FM2_1 and FM2_2, between FM1_3 and FM1_4, between the different mirrors constituting the hollow corner cube in each arm of the interferometer or between the input and output pick-off mirrors. Sufficient space was provided under the corner cube mirrors to allow for the translation stage, and to prevent mechanical interference between the lower folding mirrors and the base plate.

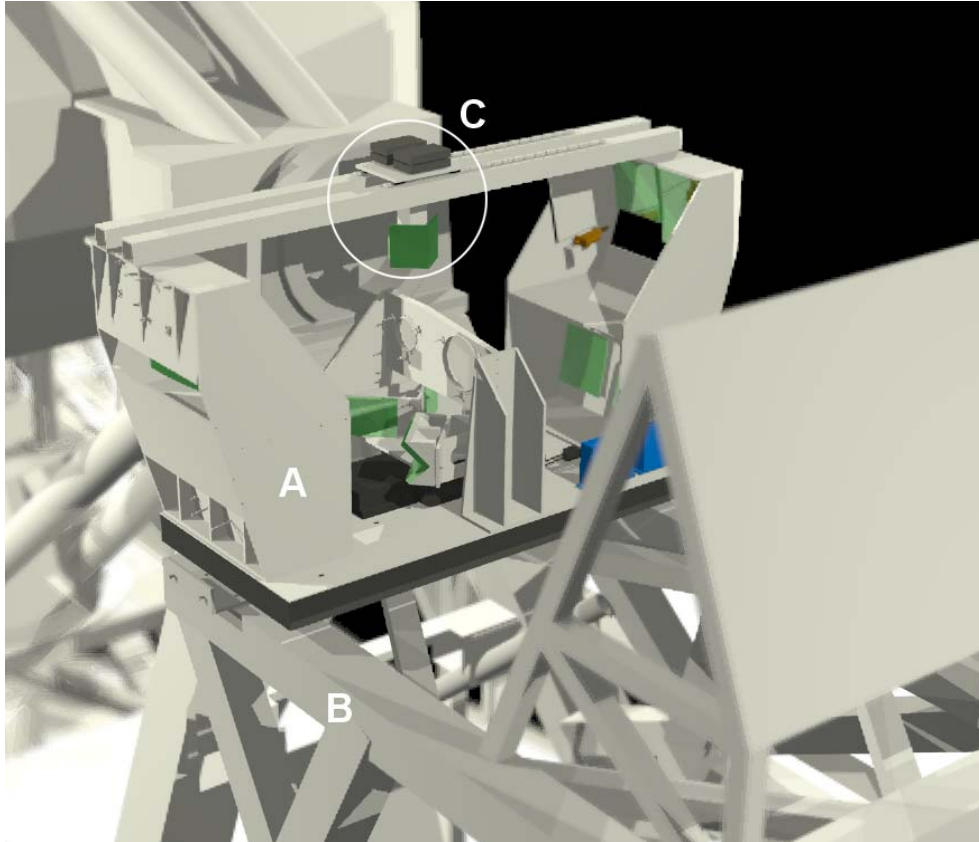


Fig. 2. A simplified view of the IFTS optics and base plate (A) at the mounting location on the telescope structure (B). A pickoff mirror assembly (C) allows SCUBA-2 to be used without the IFTS.

Symmetry in the Mach-Zehnder design⁵ of the IFTS allows the optical design to be simplified by considering only one half of the interferometer and then mirroring the resulting optics about the beamsplitter plane for the other half, as shown in Fig. 4. The two input ports are placed side by side in the SCUBA-2 intermediate image plane; the input beams are fed into the spectrometer by two pick-off mirrors and returned to the SCUBA-2 beam by two corresponding output mirrors.

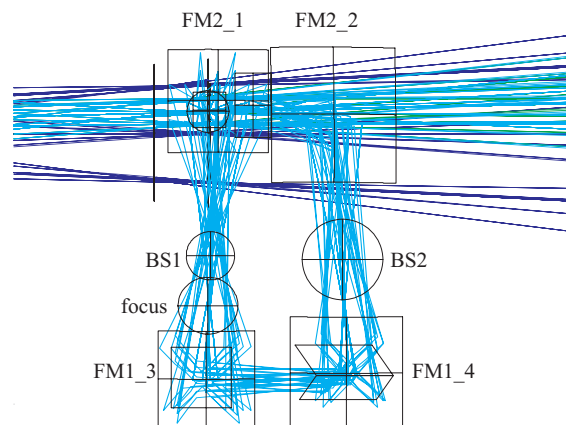


Fig. 3. Side view of the IFTS optics, showing the clearance around the beam splitters and the space between the folding mirrors.

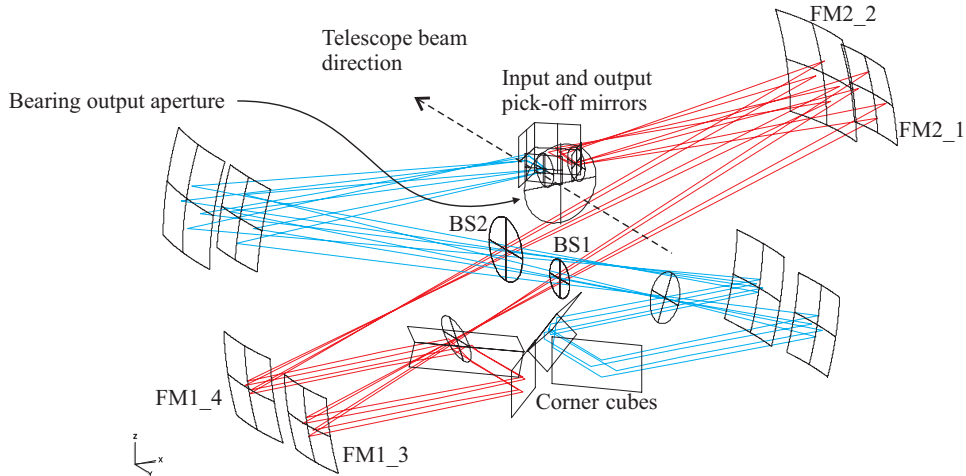


Fig. 4. View of the symmetrical nature of the IFTS. Rays for the central field point for the two arms of the interferometer are shown, along with the corresponding input and output beam splitters (BS1 and BS2, respectively), and the two corner cubes that are attached to the same translation stage.

3. RESULTS

Optimizing the FOV and spectral resolution within the constraints imposed by the fixed space envelope was a significant challenge. In the sections below we present the results of the optimization and discuss the impact of the design in terms of the effect on the FOV, spot patterns, vignetting, beam footprints as a function of increasing optical retardation within the interferometer (i.e. spectral resolution) and final prescriptions for the mirror surfaces.

Field Of View

SCUBA-2 has a nominal 8'x8' FOV. At the detector image plane, 1' corresponds to 11.84 mm. The pixels themselves are 1.055 mm in diameter and are spaced on a 1.135 mm grid. It is not possible to pass the entire FOV through the interferometer due to the size of the beam at the IFTS mounting location; the maximum achievable FOV for each port of FTS-2 is ~ 9 arcmin², roughly corresponding to one quadrant of the SCUBA-2 FOV. The layout of the FTS-2 output ports on the SCUBA-2 focal plane is shown in Fig. 5. (A discussion of how the two input ports are used to provide atmospheric cancellation is presented elsewhere.³) In addition to the reduced FOV, FTS-2 also introduces flips in the image coordinates relative to the normal SCUBA-2 image, due to the parity of reflections within the IFTS. The image coordinate transform between the case with the camera alone and the case with the addition of the FTS is shown in Fig. 5, Table 1 and Table 2.

With the spectrometer in use, the image is distorted and very slightly rotated relative to the normal SCUBA-2 image, due to the horizontal tilt of the FM2_2 folding mirror along its Y axis. This tilt was introduced to position the output pick-off mirrors as close as possible to the input pick-off mirrors, in order to limit the vignetting and reduce the instrument's volume.

3.1 Spot Patterns

At ZPD, the rays from each arm of the IFTS are perfectly superimposed for all field points in the FOV. As the interferometer optical path varies, however, the field points for the two ports diverge. The spot size and position on the image plane for each field was calculated, and the superposition of the two images coming from the two arms of the interferometer was analyzed over a range of interferometer optical path difference. With increasing path difference, the spots coming from the two arms of the interferometer for a particular field change shape and increase in size, and also shift slightly away from each other and away from their ideal ZPD position. This effect grows larger with off-axis distance; there is no interference modulation at the port periphery for travel distances greater than ~ 75 mm, since the image shift is larger than the pixel size, as can be seen in Fig. 6. The vignetting at the FOV periphery also increases with increasing travel distance, as a consequence of the limited size of the powered mirrors within the interferometer. The variation of spot size, spot position and vignetting for each field and for various travel distances is analyzed in more detail in the following sections.

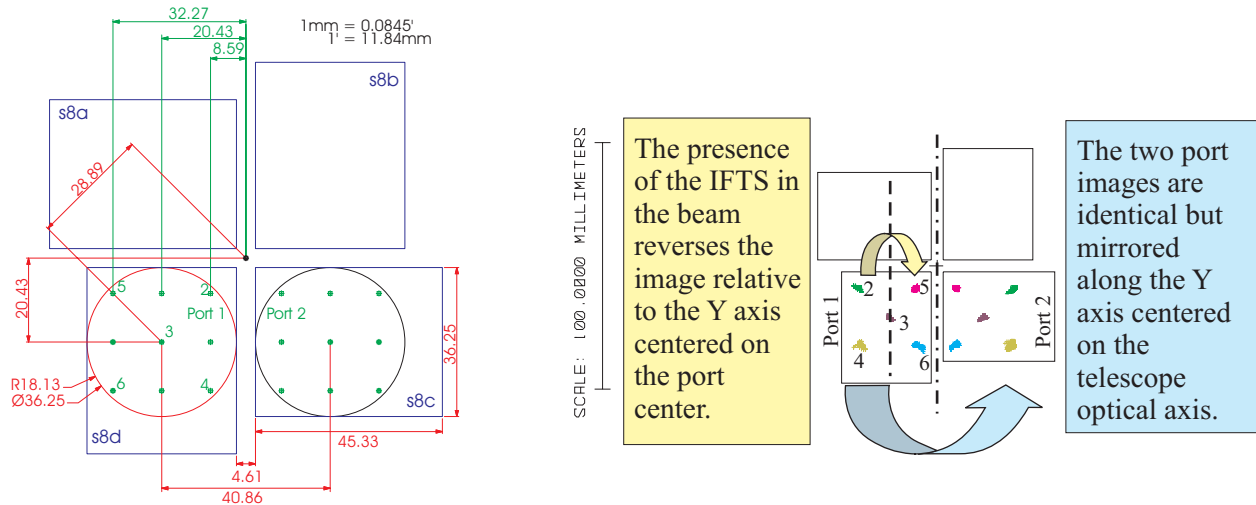


Fig. 5. Left: A schematic of the 8'x8' telescope FOV and the footprints of the four SCUBA-2 detector sub-arrays (rectangles). Only the 850 μm detector array is shown; the 450 μm layout is similar. The FOV of the two ports of IFTS are shown as circles, with the array of SCUBA-2 field points without the IFTS shown as dots. Right: A schematic of the coordinate transform between the normal SCUBA-2 image coordinates and those when IFTS-2 is in use.

Table 1. Angular field coordinates used to model the two IFTS input ports in Zemax.

Field Point	FTS-2 Field #	Port #1		Port #2	
		X (degrees)	Y (degrees)	X (degrees)	Y (degrees)
Telescope Optical axis	1	0	0	0	0
Port center	3	-0.02876	-0.02876	0.02876	-0.02876
Corners of 2' square around center	2	-0.01209	-0.01209	0.01209	-0.01209
	4	-0.01209	-0.04543	0.01209	-0.04543
	5	-0.04543	-0.01209	0.04543	-0.01209
	6	-0.04543	-0.04543	0.04543	-0.04543

Table 2. Field coordinates at the focal plane for the FTS-2 FOV.

Field Point	FTS-2 Field #	SCUBA-2 Field #	Port #1		Port #2	
			X (mm)	Y (mm)	X (mm)	Y (mm)
Telescope Optical axis	1	1	0	0	0	0
Port center	3	3	-20.0323	-20.0308	20.0323	-20.0308
Corners of 2' square around center	2	5	-31.7310	-8.3586	31.7310	-8.3586
	4	6	-31.7105	-32.0246	31.7105	-32.0246
	5	2	-8.4241	-8.5459	8.4241	-8.5459
	6	4	-8.3773	-32.2412	8.3773	-32.2412

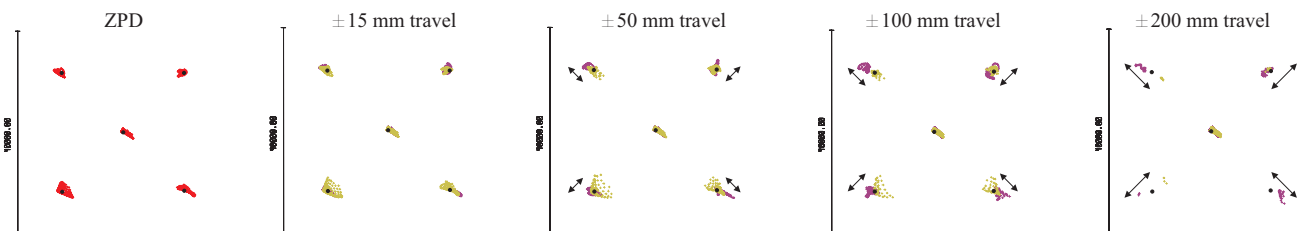


Fig. 6. Superposition of the spots for the two arms of the interferometer, for FTS-2 port #1. The spots corresponding to the normal SCUBA-2 image are shown as black circles and define the ideal spot positions at ZPD. Spots from the two arms of the interferometer are coincident at ZPD (left) but are seen to move away from each other and from the ideal position as a function of mirror travel distance, especially at the periphery of the FOV. The amplitude of the shift is represented by arrows. The vignetting at the FOV periphery also increases with increasing travel distance.

Spot size across the FTS-2 FOV increases with travel distance, but stays under diffraction limit for travel between +200 mm and -100 mm as shown in Table 3. The cases where the spot size is greater than the SCUBA-2 Airy radius are indicated in gray.

Table 3. RMS Spot radius (μm) vs. field of view and travel distance

Field #	2 (corner)	3 (port center)	4 (corner)	5 (corner)	6 (corner)	
FOV (deg.)	0.01711198	0.04072935	0.04698478	0.04698478	0.0642053	Airy Radius (μm)
SCUBA-2 RMS spot radius (μm)	133.51	146.92	167.79	122.040	148.67	2820
Travel (mm)	RMS spot radius (μm) referenced on chief ray					
200	1278.53	763.15	1519.94	2303.04	2574.04	2914
150	806.49	779.85	996.05	1051.42	1209.62	2870
100	778.35	798.99	1052.66	1214.97	1006.35	2827
50	562.32	822.46	930.40	836.87	1129.04	3788
15	780.40	835.56	1016.31	562.85	1061.97	3630
0	983.13	841.09	1252.08	610.48	1089.92	3591
-15	1015.77	846.36	1436.71	714.62	1136.45	3556
-50	903.07	853.28	1575.29	857.15	1305.42	3447
-100	2184.03	855.31	2864.79	1332.28	2219.53	3403
-150	5752.90	864.65	8149.83	3570.26	5222.3	3405
-200	1.10E+04	873.98	2.10E+04	7681.65	1.10E+04	3331

3.2 Beam footprints

Footprints for the beams within the IFTS were computed at each surface. Figures 7 and 8 show the footprints, including vignetting effects. The footprints at surfaces after FM1_3 vary with the corner cube travel distance. The beam footprint on the corner cubes for travel distances between -200 mm and +200 mm is shown in Fig. 9. The pupil is located roughly at the corner cube apex at ZPD, and is stationary relative to the input beamsplitter. Beam footprints for the surfaces after the corner cubes are shown in Fig. 10.

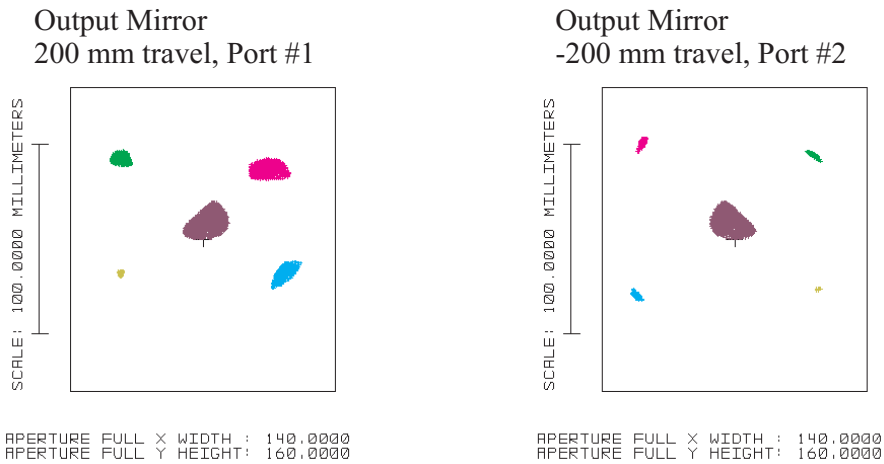


Fig. 7. Footprint of the vignettted beam at the output pick-off mirrors.

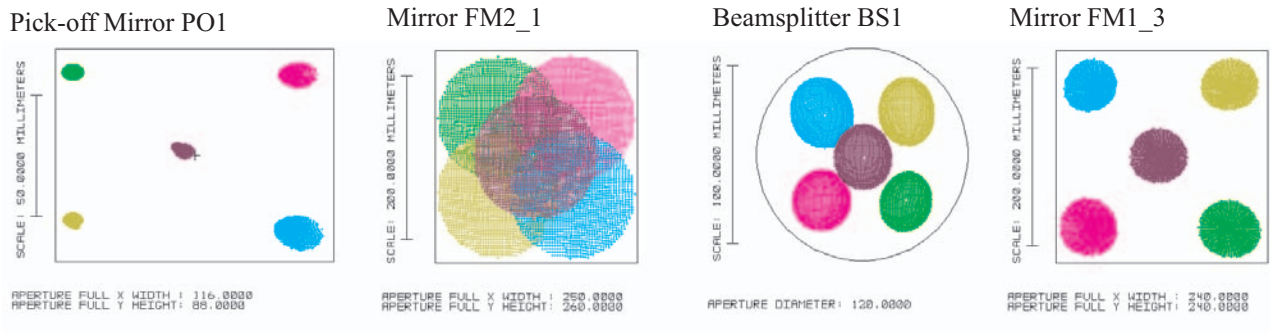


Fig. 8. Beam footprints for surfaces between from input pick-off mirror PO1 up to folding mirror FM1_3.

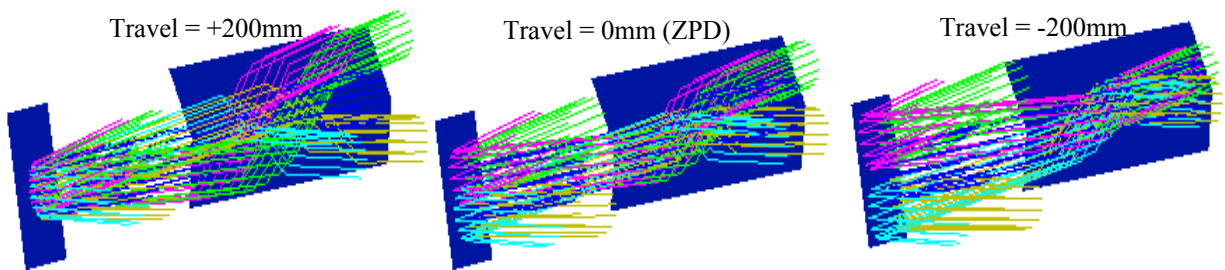


Fig. 9. Beam footprint at the corner cubes

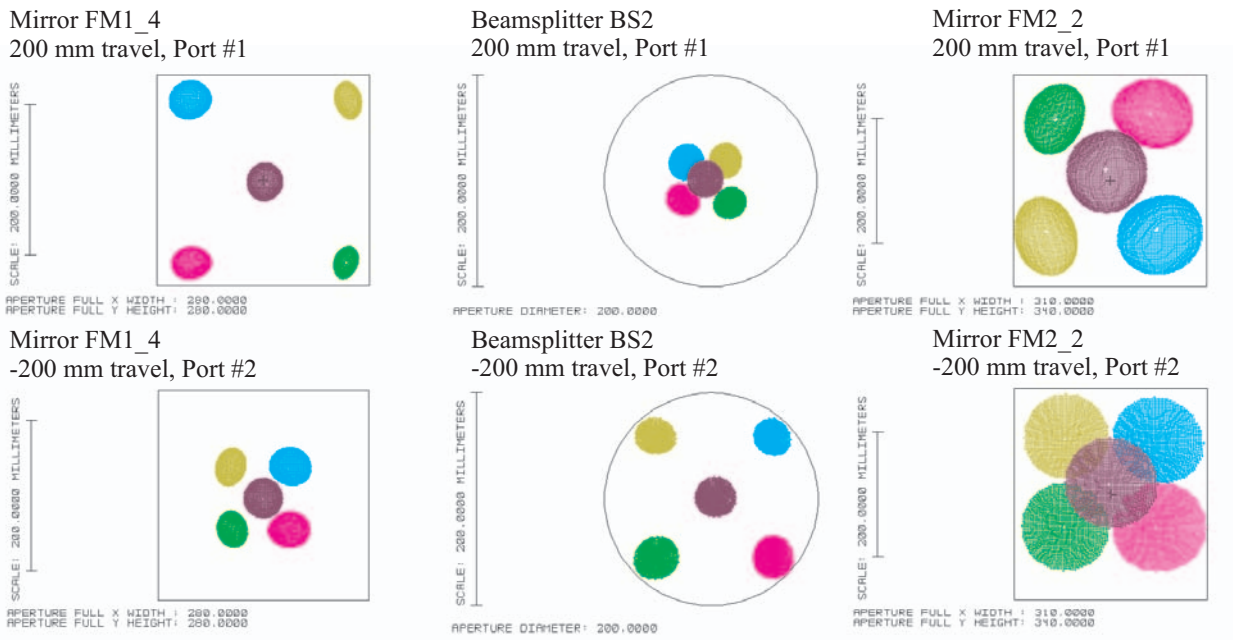


Fig. 10. Beam footprints at mirrors after FM1_3

3.3 Vignetting

Spill-over and vignetting effects at the various surfaces in the FTS, camera and telescope were studied in detail. The spill-over occurs mainly at the camera cold stop and at the output pick-off mirrors, at ± 200 mm travel, as shown in Fig. 11 and Fig. 12. While there is no other spill-over in the IFTS except at the output pick-off mirror at 200 mm travel (as shown in Fig. 12), there is spill-over at other surfaces after the IFTS, namely N1, N2, the cryostat window, and N5, as shown in Fig. 13.

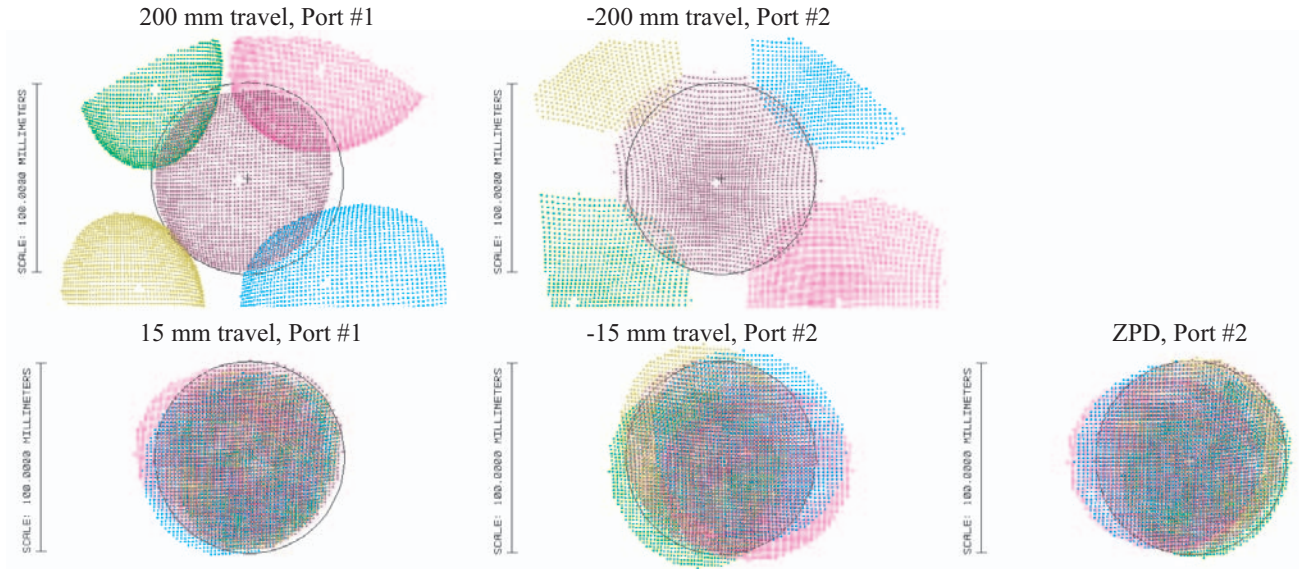


Fig. 11. Spillover at the camera cold stop

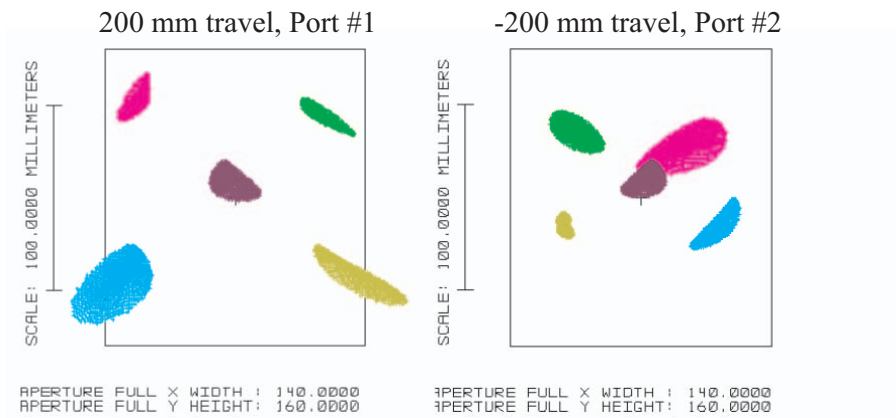
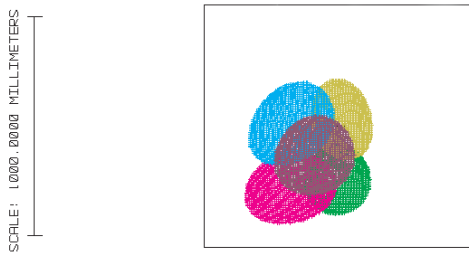


Fig. 12. Spillover at the IFTS output pick-off mirrors

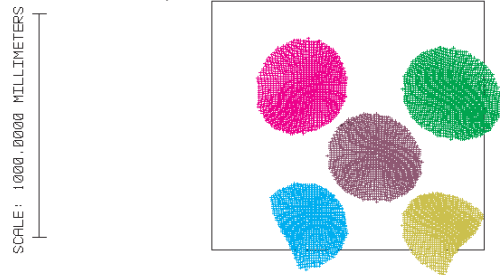
Vignetting as a result of spill-over at surfaces between the bearing output and the detector plane increases with travel distance. For each field, the proportion of rays getting through each arm of the interferometer was compared, and the maximum achievable contrast for various travel distances was computed. Shift between the two spots from the two arms of the interferometer was not considered when calculating this maximum achievable contrast. To compute the real image contrast obtained at each point of the image, the shift between the two spots coming from the two arms of the interferometer must be known. If the shift is greater than the Airy radius, there will be no interference between the two spots. Therefore, the shift between the two spots coming from the two arms of the interferometer for each field was computed. Cases for which the shift is greater than the SCUBA-2 Airy radius are shown in gray in Table 4.

Mirror N1
200 mm travel, Port #1



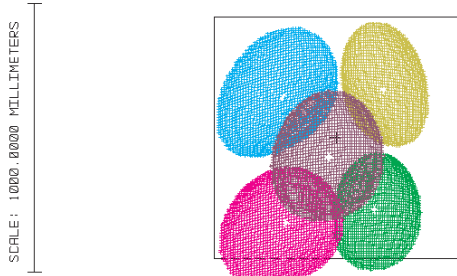
APERTURE FULL X WIDTH : 1076.0000
APERTURE FULL Y HEIGHT : 1109.0000

Mirror N1
-200 mm travel, Port #2



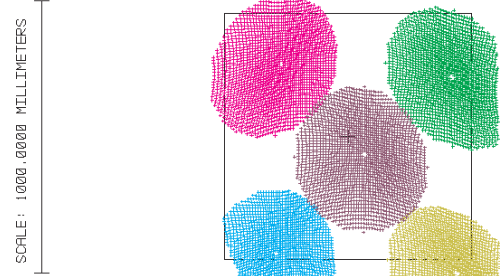
APERTURE FULL X WIDTH : 1076.0000
APERTURE FULL Y HEIGHT : 1109.0000

Mirror N2
200 mm travel, Port #1



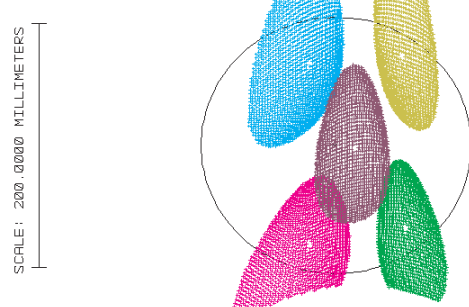
APERTURE FULL X WIDTH : 800.0000
APERTURE FULL Y HEIGHT : 900.0000

Mirror N2
-200 mm travel, Port #2



APERTURE FULL X WIDTH : 800.0000
APERTURE FULL Y HEIGHT : 900.0000

Cryostat Window
200 mm travel, Port #1



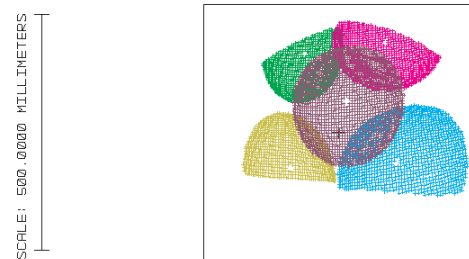
APERTURE FULL X WIDTH : 210.0000
APERTURE FULL Y HEIGHT : 210.0000

Cryostat Window
-200 mm travel, Port #2



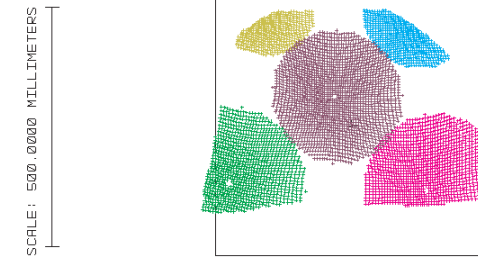
APERTURE FULL X WIDTH : 210.0000
APERTURE FULL Y HEIGHT : 210.0000

Mirror N5
200 mm travel, Port #1



APERTURE FULL X WIDTH : 540.0000
APERTURE FULL Y HEIGHT : 540.0000

Mirror N5
-200 mm travel, Port #2



APERTURE FULL X WIDTH : 540.0000
APERTURE FULL Y HEIGHT : 540.0000

Fig. 13. Spillover at N1, N2, at the cryostat window and at N5

Table 4. Field coordinates at the array and proportion of rays getting through to the detector for the IFTS port #1

Field (deg.)	Absolute travel distance (mm)	Contrast excluding image shift	Proportion of rays getting through to the detector		Shift between two spots from two arms of the IFTS (mm)	Chief ray image plane coordinates (mm)			
			Side with increasing mirror travel	Side with decreasing mirror travel		Positive travel		Negative travel	
						X	Y	X	Y
Central field #3 (-0.02876, 0.02876)	0	1.000	97.55%	97.55%	0.000	-19.235	-20.650	-19.235	-20.650
	15	0.991	98.01%	97.14%	0.005	-19.235	-20.647	-19.236	-20.652
	50	0.977	98.83%	96.53%	0.017	-19.233	-20.642	-19.238	-20.658
	100	0.970	91.64%	94.44%	0.034	-19.230	-20.634	-19.239	-20.667
	150	0.995	91.64%	91.22%	0.052	-19.227	-20.626	-19.240	-20.676
	200	0.999	91.64%	91.69%	0.069	-19.224	-20.619	-19.240	-20.686
Field #2 (-0.01209, 0.01209)	0	1.000	95.41%	95.41%	0.000	-32.082	-8.501	-32.082	-8.501
	15	0.859	99.75%	85.67%	0.311	-32.194	-8.474	-31.901	-8.579
	50	0.656	98.32%	64.51%	1.212	-32.257	-8.533	-31.145	-9.015
	100	0.523	71.44%	37.38%	3.596	-32.128	-8.664	-29.020	-10.473
	150	0.363	43.45%	15.76%	8.363	-32.186	-8.412	-25.337	-13.211
	200	0.153	19.07%	2.91%	16.664	-32.983	-7.219	-19.816	-17.433
Field #4 (-0.01209, 0.04543)	0	1.000	98.27%	98.27%	0.000	-31.039	-32.308	-31.039	-32.308
	15	0.899	99.59%	89.55%	0.822	-31.115	-32.266	-30.293	-32.292
	50	0.798	84.19%	67.16%	0.854	-31.227	-32.034	-30.381	-31.916
	100	0.710	53.85%	38.25%	3.502	-31.546	-31.723	-28.448	-30.090
	150	0.489	26.93%	13.16%	10.667	-32.500	-31.956	-23.893	-25.655
	200	0.281	1.99%	0.56%	27.854	-34.522	-33.286	-12.973	-15.637
Field #5 (-0.04543, 0.01209)	0	1.000	86.23%	86.23%	0.000	-8.041	-8.526	-8.041	-8.526
	15	0.880	91.02%	80.06%	0.380	-8.153	-8.703	-7.969	-8.371
	50	0.721	88.73%	64.00%	1.071	-8.505	-9.125	-8.011	-8.175
	100	0.626	65.53%	41.05%	0.915	-9.001	-9.458	-8.783	-8.569
	150	0.453	42.53%	19.28%	2.017	-9.068	-8.972	-10.680	-10.184
	200	0.177	22.74%	4.03%	8.713	-8.102	-6.990	-13.955	-13.444
Field #6 (-0.04543, 0.04543)	0	1.000	88.37%	88.37%	0.000	-7.364	-32.231	-7.364	-32.231
	15	0.885	92.20%	81.64%	0.209	-7.267	-32.216	-7.476	-32.216
	50	0.785	82.56%	64.81%	0.835	-7.042	-32.134	-7.864	-31.988
	100	0.622	57.89%	42.02%	2.789	-6.512	-32.150	-8.995	-30.879
	150	0.524	36.41%	19.07%	7.406	-5.425	-32.695	-11.341	-28.240
	200	0.132	16.57%	2.19%	16.554	-3.464	-34.150	-15.802	-23.113

3.4 Mirror surface prescriptions

The mirror surface prescriptions are detailed in the Table 5 and 6 below. The size of each mirror was optimized considering the vignettted beam footprint.

Table 5. Aperture size and decenter for each mirror surface on one arm of the interferometer

Surface	Aperture size (mm)		Aperture decenter (mm)	
	Width (X)	Height (Y)	X *	Y
PO1	116	88	5	-4
FM2_1	250	260	25	-28
FM1_3	240	240	-4	10
CC1	270	106		
CC2	270	85		
CC3	210	150		
FM1_4	280	280	10	-5
FM2_2	310	340	-21	6
PO2	140	160	1	-15
	Diameter		X *	Y
BS1	120		6	-5
BS2	200		0	4

* The sign is reversed for the equivalent mirror on the other side of the IFTS.

The pick-off and corner cube mirror surfaces are flat; all other folding mirrors are extended polynomial surfaces, described by the following equation:

$$z = \frac{cr^2}{1 + \sqrt{1 - (1+k)c^2r^2}} + \sum_{i=1}^N A_i E_i(x, y) \quad (1)$$

where $c = \frac{1}{R}$, and where $E_1 = x$, $E_2 = y$, $E_3 = x^2$, $E_4 = xy$, $E_5 = y^2$, $E_6 = x^3$, $E_7 = x^2y$, $E_8 = xy^2$, $E_9 = y^3$

Table 6. Extended polynomial parameters for each mirror surface on one « side » of the interferometer (port #1)

Surface	FM2_1	FM1_3	FM1_4	FM2_2
R	-1239.388	1135.457	1188.090	-1173.798
k	-0.669	2.379	-2.367	2.132
A ₁	0	0	0	0
A ₂ *	0	0	0	0
A ₃	-7.86e-6	5.161e-6	6.626e-6	1.945e-6
A ₄ *	3.224e-6	1.407e-6	-2.320e-7	-9.790e-6
A ₅	3.605e-6	-1.780e-6	8.613e-7	4.362e-6
A ₆ *	3.080e-8	6.144e-8	-4.080e-9	-6.530e-8
A ₇	-4.750e-8	3.706e-8	4.178e-8	-1.960e-7
A ₈ *	3.608e-8	-2.470e-8	-4.990e-9	-2.220e-8
A ₉	-4.480e-8	9.553e-9	1.434e-8	-2.490e-8

* The sign is reversed for the equivalent mirror on the other side of the IFTS.

4. CONCLUSION

Designing a spectrometer for use with SCUBA-2 has proven to be a challenging problem. A Fourier spectrometer was selected because of its high throughput, intermediate resolution, broad spectral coverage and inherent wavelength calibration. The optical design problem for FTS-2 was essentially to reproduce the original image and pupil at the outputs of the interferometer, while maintaining unity magnification, in order to allow the instrument to be placed midway through the existing SCUBA-2 feed optics. The optical design was complicated by the limited available space, the curved image surface at the input, and the $\sim f/7$ input beam. It was impossible to achieve diffraction limited imaging at high spectral resolution over the entire SCUBA-2 field of view. The final design represents the best trade-off between FOV and spectral resolution, considering the constraints imposed by the fixed space envelope. We believe the resulting instrument will achieve optimal performance considering all the design constraints.

REFERENCES

1. Holland, W.S., Robinson, E.I., Gear, W.K., Cunningham, C.R., Lightfoot, J.F., Jenness, T., Ivison, R.J., Stevens, J.A., Ade, P.A.R., Griffin, M.J., Duncan, W.D., Murphy, J.A. and Naylor, D.A., "SCUBA: a common-user submillimetre camera operating on the James Clerk Maxwell Telescope", *Mon. Not. R. Astron. Soc.* **303**, 659-672 (1999).
2. Holland, W.S., Duncan, W.D., Kelley, B.D., Irwin, K.D., Walton, A.J., Ade, P.A.R., and Robson, E.I., "SCUBA-2: A large format submillimetre camera on the James Clerk Maxwell Telescope", *Proc. SPIE, Millimeter and Submillimeter Detectors for Astronomy* **4855**, 1-18 (2003).
3. B. G. Gom D. A. Naylor, "An update on the imaging Fourier transform spectrometer for SCUBA-2", *Proc. SPIE, SPIE Europe International Symposium Astronomical Telescopes*, Paper 5498-86 (2004).
4. D. A. Naylor and B. G. Gom, "FTS-2: A Submillimetre Astronomical Imaging Fourier Transform Spectrometer", FTS topical meeting, Santa Fe, New Mexico, (February 2007).
5. Ade, P.A.R, Hamilton, P.A., and Naylor, D.A., "An Absolute Dual Beam Emission Spectrometer", *Optical Society of America, FTS topical meeting*, poster FWE3, Santa Barbara, California, (1999).